Geomech. Geophys. Geo-energ. Geo-resour. (2024) 10:107
https://doi.org/10.1007/s40948-024-00793-7

ORIGINAL ARTICLE

Effect of swab and surge pressure on the time-dependent wellbore natural fracture development

Arnaud Regis Kamgue Lenwoue · Zhonghui Li · Pengjie Hu · Naomie Beolle Songwe Selabi · Lesly Dasilva Wandji Djouonkep

Received: 17 November 2021 / Accepted: 7 April 2024 / Published online: 14 June 2024

Abstract Drilling engineers continue to grapple with the persistent challenge of maintaining wellbore stability. Throughout the drilling process, the wellbore pressure experiences fluctuations induced by various factors such as swab and surge pressure, leading to potential instability. This study employs a numerical approach, utilizing Abaqus software, to investigate the impact of swab and surge pressure on the natural fracture growth within the wellbore and the evolving pore pressure. A computational tool developed with MATLAB is then utilized to ascertain a safe operational mud window by assessing the time-dependent collapse and fracture pressures. The findings illustrated a notable increase in fracture width as a function of time in response to swab and surge pressure, with the most significant percentage increase reaching 69.92%. Notably, a 69.16% augmentation in fracture width is observed in the immediate vicinity of the wellbore following the application of swab and surge pressure. However, parameters such as fracture length, loss circulation rate, and pore fluid pressure exhibited marginal changes post-integration of swab and surge effects. The examination of the time-dependent wellbore stability after integration of swab and surge pressure indicated a narrowing of the initial mud window as a function of time, with a 14.33% increase in collapse pressure and a 13.80% decrease in fracture pressure. The numerical model verification against analytical solutions demonstrated good agreement, highlighting its potential utility in optimizing particle size for wellbore reinforcement and mitigating lost circulation through natural fracture sealing.

Article highlights

- Fracture width as a function of time profiles increased with the swab and surge pressure;
- Swab and surge pressure weakly affected the fracture length, loss circulation and the pore pressure;
- Safe mud window narrowed with the time after integration of swab and surge pressure.

A. R. Kamgue Lenwoue (✉) · Z. Li (✉) · P. Hu
School of Petroleum Engineering, National Engineering Research Center for Oil & Gas Drilling and Completion Technology, Yangtze University, Wuhan 430100, Hubei, China
e-mail: regiskamgue@yahoo.fr

Z. Li
e-mail: lizhonghui@yangtzeu.edu.cn

A. R. Kamgue Lenwoue · Z. Li · P. Hu
Hubei Key Laboratory of Oil and Gas Drilling and Production Engineering, Yangtze University, Wuhan 430100, Hubei, China

N. B. Songwe Selabi
School of Materials and Metallurgy, Wuhan University of Science and Technology, Wuhan, China 430081

L. D. Wandji Djouonkep
School of Petroleum Engineering, Applied Chemistry in Oil and Gas Fields, Yangtze University, Wuhan 430100, China

Keywords Swab and surge pressure · Time-dependent · Natural fracture development

Abbreviations

c_T, c_B	Leak off coefficients respectively at the top and the bottom of the fracture (m/s/Pa)
c_l	Fluid loss coefficient
CZM	Cohesive Zone Model
g	Gravitational acceleration (m/s^2)
PKN	Perkins–Kern–Nordgren
P_1, P_2	Pipe element nodes
ΔP	Pressure difference between P_1 and P_2 (Pa)
q_f	Longitudinal flow rate per unit of width (m^2/s)
T	Total simulation time (s)
t_n, t_{s1}, t^0_{s2}	Normal nominal stress, First and second shear nominal stress respectively (Pa)
t^0_n, t^0_{s1}, t^0_{s2}	Normal nominal stress, First and second shear nominal stress peak values respectively (Pa)
v_t, v_b	Normal velocities respectively at the top and the bottom of the fracture (m/s)
V	Fluid velocity (m/s)
w	Fracture aperture (m)
ΔZ	Elevation difference (m)
ρ	Drilling fluid density (kg/m^3)

1 Introduction

Excessive fluctuations in wellbore pressure pose significant challenges, leading to various instabilities such as lost circulation, formation fracturing, kick issues, and wellbore collapse, as documented by Cannon (1934), Horn (1950), and Goins et al. (1951). Among these fluctuations, swab and surge pressures stand out as primary contributors, with Kong et al. (2014) reporting that 25% of drilling complications stem from surge pressures. Previous research has extensively explored the impact of these pressures. Crespo et al. (2012) developed a Yield Power Law model to analyze surge and swab pressures, emphasizing the influence of factors like pipe velocity and yield stress. Similarly, Srivastav et al. (2012) conducted laboratory experiments highlighting the significance of drill pipe eccentricity, annular clearance, and fluid rheology on swab surge pressure. Kong et al. (2014) found that surge pressure escalated with drill pipe speed while decreasing with gas influx rate and wellbore diameter. Tang et al. (2014) and Tikhonov et al. (2016) further explored factors affecting pressure modeling, including well eccentricity and hydraulic losses.

Despite these extensive researches, few studies have directly addressed the impact of swab and surge pressures on wellbore stability. Zamanipour et al. (2016) observed transient surge pressure-induced stress variations, while Zhang et al. (2018) focused on near wellbore stress and pore pressure effects. More recently, Meng et al. (2019a, b) developed a model to compute minimum mud density required for stability amidst swab/surge fluctuations, highlighting disparities with conventional methods. Past studies primarily focused on predicting swab and surge pressures using steady and unsteady models (Burkhadt 1961; Lubinski et al. 1977; Mitchell 1988), or identified factors influencing pressure calculation (Crespo et al. 2012; Tang et al. 2014; Abduljabbar et al. 2018). Those integrating these pressures with wellbore stability analysis mainly explored stress distribution or near wellbore pore pressure effects. Few have investigated how swab and surge pressures impact parameters of naturally fractured formations, crucial for maintaining stability.

To address these gaps, this study employs a plane strain poroelastic finite element analysis to examine swab and surge pressure effects on natural fracture development and time-dependent wellbore stability. Abaqus software is first utilized to conduct numerical simulations and investigate the influence of the swab and surge pressure on fracture growth and pore pressure. Then, a MATLAB program is used to assess the time-dependent safe mud window. The results are validated against analytical solutions, offering insights into mitigating wellbore instability amidst pressure fluctuations.

2 Theory

The aims of this study are to investigate the impact of swabbing and surge pressure on the expansion of natural fractures within the wellbore, as well as the time-sensitive threshold for safe mud operations. This section will outline the fundamental equations governing these phenomena.

2.1 Governing equations of hydraulically driven fracture

The numerical simulation of the influence of swabbing and surge pressure on wellbore natural fracture growth encompasses the subsequent phenomena:

(a) Circulation of drilling fluid within the wellbore;
(b) Initiation and advancement of fractures alongside fracturing fluid movement;
(c) Deformation of porous medium and flow of pore fluid.

2.1.1 Fluid flow inside the wellbore

The drilling fluid's flow within the wellbore is replicated through the pipe element model in Abaqus. This model relies on Bernoulli's equation, with its governing equation provided as per (Simulia 2016):

$$\Delta P = \rho g \Delta Z + C_l \frac{\rho V^2}{2} \tag{1}$$

where, ΔP represents the pressure disparity between two nodes P_1 and P_2 of the pipe element, Pa; ρ is the density of the drilling fluid, kg/m^3; g is the gravitational acceleration, m/s^2; ΔZ is the vertical displacement between the nodes P_1 and P_2, m; V is the fluid velocity in the pipe, m/s; C_l stands for the fluid loss coefficient.

2.1.2 Fracture propagation and fracturing fluid flow

The Abaqus coupled pressure/deformation cohesive zone model is employed to simulate fracture propagation and fracturing fluid flow. In this study, damage initiation is assumed to occur when the following quadratic stress criterion is satisfied, as proposed by Wu et al. (2018):

$$\left(\frac{\langle t_n \rangle}{t_n^0}\right)^2 + \left(\frac{t_{s1}}{t_{s1}^0}\right)^2 + \left(\frac{t_{s2}}{t_{s2}^0}\right)^2 = 1 \tag{2}$$

where, t_n, t_{s1} and t_{s2} are respectively the normal nominal stress, the first shear and second shear nominal stress, Pa; t_n^0, t_{s1}^0 and t_{s2}^0 respectively represent their peak values, Pa. The constitutive equations governing the flow of fracturing fluid are derived from Reynolds' lubrication theory and are provided by Zielonka et al. (2014):

$$\frac{\partial w}{\partial t} + \frac{\partial q_f}{\partial s} + v_t + v_b = 0 \tag{3}$$

where, w is the fracture aperture, m; q_f is the longitudinal flow rate per unit of width, m^2/s; v_t and v_b respectively represent the normal velocities of the fluid flow at the top and the bottom of the fracture, m/s.

2.1.3 Porous medium deformation and pore fluid flow

The porous medium deformation is controlled by Biot's theory of poroelasticity, while pore fluid flow is elucidated through the continuum equation and Darcy's theory. The governing equations for these processes have been comprehensively detailed in numerous studies (Fjaer et al., 2008; Jaeger et al. 2009; Zielonka et al. 2014; Feng and Gray 2018a, b, c). Hence, these equations will not be reiterated in the current research.

2.2 Governing equations of time-dependent wellbore stability analysis

The time-dependent wellbore stability model developed in this study follows a similar methodology to the model proposed by Rahman et al. (2000). The mechanical properties of the rock formation, such as Young's modulus and Poisson's ratio, are assumed to remain constant throughout the simulation. The variation in pore pressure over time is considered as the sole factor influencing the time-dependent nature of wellbore stability. The time-dependent pore fluid pressure, denoted as p(t), is directly derived from the newly developed numerical model using finite element Abaqus software.

2.2.1 Stress and pore fluid pressure as a function of time in cylindrical coordinate system

A MATLAB program is developed to analytically compute the time-dependent stress distribution in the cylindrical coordinate system. The equations governing wellbore stability, incorporating the

time-dependent wellbore pressure, are presented as follows, based on Fjaer et al. (2008):

$$\sigma_r(t) = \frac{\sigma_x^o + \sigma_y^o}{2}\left(1 - \frac{R_w^2}{r^2}\right) + \frac{\sigma_x^o - \sigma_y^o}{2}\left(1 + 3\frac{R_w^4}{r^4} - 4\frac{R_w^2}{r^2}\right)cos2\theta + \tau_{xy}^o\left(1 + 3\frac{R_w^4}{r^4} - 4\frac{R_w^2}{r^2}\right)sin2\theta + P_w(t)\frac{R_w^2}{r^2} \quad (4)$$

$$\sigma_\theta(t) = \frac{\sigma_x^o + \sigma_y^o}{2}\left(1 + \frac{R_w^2}{r^2}\right) - \frac{\sigma_x^o - \sigma_y^o}{2}\left(1 + 3\frac{R_w^4}{r^4}\right)\cos 2\theta - \tau_{xy}^o\left(1 + 3\frac{R_w^4}{r^4}\right)\sin 2\theta - P_w(t)\frac{R_w^2}{r^2} \quad (5)$$

$$\sigma_z(t) = \sigma_z^o - \nu_{fr}\left[2\left(\sigma_x^o - \sigma_y^o\right)\frac{R_w^2}{r^2}\cos 2\theta + 4\tau_{xy}^o\frac{R_w^2}{r^2}\sin 2\theta\right] \quad (6)$$

2.2.2 Time dependent wellbore collapse pressure

The Mohr–Coulomb criterion is employed to predict shear failure in the rock formation. It is assumed that the rock collapses due to shear failure when the shear stress exceeds the shear strength of the rock. The equations, which account for the time dependency resulting from pore pressure changes over time, are provided by Rahman et al. (2000):

$$\tau(t) \geq \tau_u(t) \quad (7)$$

$$\tau(t) = \frac{\sigma_1(t) - \sigma_3(t)}{2}\cos\phi \quad (8)$$

$$\tau_u(t) = \left\{\frac{\sigma_1(t) + \sigma_3(t)}{2} - \frac{\sigma_1(t) - \sigma_3(t)}{2}\sin\phi - p(t)\right\}\tan\phi + c \quad (9)$$

$$\sigma_1(t) = \max\left(\sigma_r(t), \sigma_\theta(t), \sigma_z(t)\right) \quad (10)$$

$$\sigma_3(t) = \min\left(\sigma_r(t), \sigma_\theta(t), \sigma_z(t)\right) \quad (11)$$

The parameters ϕ and c in Eq. 8 and Eq. 9 respectively represent the Mohr–Coulomb friction angle and the cohesion strength of the rock.

2.2.3 Time-dependent wellbore pressure

The failure in tensile mode occurs when the tensile strength of the rock is exceeded by the minimum effective principal stress. This condition is expressed as:

$$\sigma_3(t) - p(t) \leq -\left|\sigma_t\right| \quad (12)$$

where, $\sigma_3(t)$ is the time dependent minimum principal stress, MPa; $p(t)$ is the time dependent pore pressure and σ_t is the rock formation tensile strength, MPa.

3 Numerical modeling

3.1 Geometry and material properties

The schematic of the numerical model is illustrated in Fig. 1.

The wellbore and drill string annulus are oriented in the Z-direction but modeled in the Y-direction for better visualization. Natural fractures open in the horizontal X–Y plane. The model includes the wellbore, rock formation, and natural fractures. The wellbore radius is 0.1 m and extends from the surface to 1000 m. By considering the model symmetry, only half of the formation is represented with a 2D geometry. The input parameters for simulating sandstone rock are provided in Table 1. The formation employs coupled pore fluid stress and plane strain elements (CPE4P elements). Sh_{max} and Sh_{min} represent the maximum and minimum horizontal stresses in the x- and y-directions, respectively. The fracture follows the Perkins-Kern-Nordgren (PKN) theory with an initial length of 0.5 m and a width of 2×10^{-4} m. Due to fluctuating wellbore pressure from swabbing and surging, the fracture will reopen, with its tip propagating following the Cohesive Zone Model (CZM) in the direction of maximal horizontal stress. Two-dimensional pore pressure cohesive elements (COH2D4P) simulate the CZM. The initial pore pressure within the natural fracture is 10 MPa. The drill pipe is modeled using 2-node linear fluid pipe connector elements (FPC2D2), while the wellbore

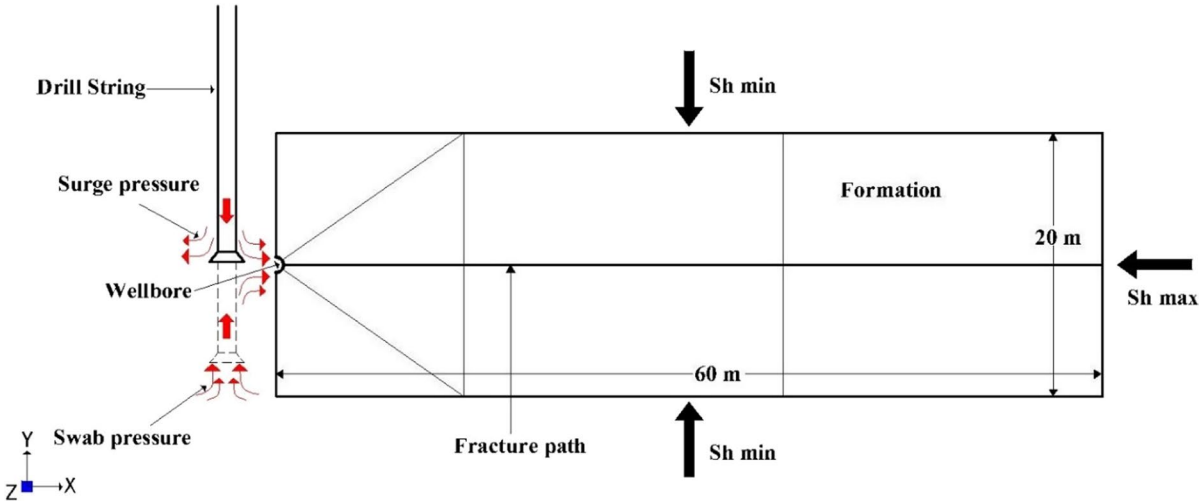

Fig. 1 Schematic of the numerical model

Table 1 Input parameters for simulation of the influence of swab and surge pressure on the time-dependent wellbore stability analysis

Parameters	Value	Parameters	Value
Formation size	20 m × 120 m	Gravitational acceleration	10 m /s^2
Formation depth	1000 m	Rock Young's modulus	7 000 MPa
Wellbore radius	10 cm	Rock Poisson's ratio	0.2
Drill-pipe radius	5 cm	Rock permeability	5 md
Drill collar OD	8 in	Rock porosity	0.25
Drill collar ID	3 in	Peak value of the nominal stress in the damage initiation criterion	0.4 MPa
Initial pore pressure	10 MPa	Fracture energy	28 J /m^2
Minimum horizontal stress	13 MPa	BK power law parameter	2.284
Maximum horizontal stress	15 MPa	Leak-off coefficient	5 × m/s/Pa
Cohesion	10 MPa	Interface stiffness	80 000 MPa
Friction angle	30 degrees	Pumping rate	0.36 m^3/min
Pore-fluid density	1.0 g/cm^3	Pore fluid viscosity	1 cp
Drilling-mud density	1.3 g/cm^3	Fracture pore pressure	10 MPa

annulus is modeled with 2-node linear fluid pipe elements (FP2D2).

3.2 Simulation steps

The analysis comprises two steps:

1. Initial Step: In this step, the initial pore pressure, far-field stresses, and initial void ratio are applied to the model.
2. Geostatic Step: This step aims to achieve equilibrium among the different loads applied during the initial step.

Afterward, the analysis proceeds with a transitional soil consolidation step. Here, dynamic mud circulation, swab and surge pressure, and loss circulation are simulated. An unsymmetric matrix storage is utilized in this step to enhance the convergence rate of the nonlinear solution. The incremental size of this

step varies from 1 to 10 s, with a total step time of T = 30 min.

3.3 Boundary conditions and loadings

The drilling fluid is injected in the wellbore from the node of the drill pipe lying at the surface. A periodic distributed surface load is applied on the wellbore surface to simulate the drill string swab and surge pressures. The model simulates the swab and surge pressure with a mechanical distributed surface load directly applied on the wellbore surface. The wellhead pressure is defined on the node of the wellbore annulus lying at the surface with a zero-boundary pore fluid pressure. The left edge is modeled with the X symmetry boundary condition and a zero-pore fluid pressure. The three other edges are modeled with constrained normal displacements and pore pressure equals to 10 MPa.

3.4 Mesh sensitivity analysis

A mesh sensitivity analysis was conducted to find the most appropriate mesh size for the numerical modeling. This involved systematically changing the mesh size from 0.001 mm to 10 cm and observing how it affected key output parameters like stress distribution, displacement profiles, and fracture dimensions. The results showed that small changes in mesh size didn't significantly alter the overall trends while finer meshes offered better details, especially in areas with high complexity. Finally, a combination of a coarse mesh size consisting of square blocks with a dimension of 1 cm in the region far away the wellbore and a fine mesh size with square blocks of 1 mm in the near wellbore region was utilized during the numerical modeling because it provided more accurate results with a good computational efficiency.

3.5 Swab and surge pressure modeling

Swab and surge pressure model utilized in this study is based on the method introduced by Lubinski et al. (1977). Additionally, the analytical model for dynamic swab and surge pressure is adapted from Mitchell's model (Mitchell 1988) and solved using Bergeron's method (Bergeron 1961). Various loading scenarios are defined in this research to include swab and surge pressure ranging from 0 to 10 MPa:

- Low swab and surge pressure levels, with a maximum magnitude of 0.75 MPa.
- Medium swab/surge pressure levels, ranging from 1.5 to 3 MPa.
- High swab/surge pressure levels, ranging from 6 to 9 MPa.

Figure 2 illustrates the different loading cases of swab and surge pressure over a transient period of 40 s. This transient profile, spanning 40 s, is replicated throughout the entire modeling process, covering a total simulation time of 30 min.

4 Validation model

4.1 Statement of theory and definitions

Despite the adoption of simplifying assumptions in the numerical modeling process, a lack of analytical solutions persists for fluid-driven fracture problems. Nonetheless, several researchers (Savitski and Detournay 2002; Bunger et al. 2005; Detournay et al. 2006; Garagash 2006; Peirce and Detournay 2008; Hu and Garagash 2010) have developed asymptotic solutions to predict fracture development and net fluid pressure for fractures developing in rock formations driven by Newtonian fluids. This study focuses on investigating asymptotic solutions within the storage and toughness boundary regime. Input parameters listed in Table 1 were carefully chosen to ensure that the numerical solutions obtained from Abaqus are comparable with the asymptotic solutions.

For instance, fracture geometries are maintained significantly smaller than the domain dimensions, cohesive properties are selected to ensure fracture size exceeds the cohesive zone, and permeability is defined to minimize the impact of poroelastic effects ahead of the fracture tip. Subsequently, comparisons between Abaqus numerical solutions and analytical asymptotic solutions are conducted to validate the numerical model. Under the above assumptions, the problem is solved by determining the net fluid pressure p (difference between fluid pressure inside the crack and far field stress); the fracture aperture $w(x, t)$ and the half length of the fracture (t); x is the spatial coordinate, t is the time.

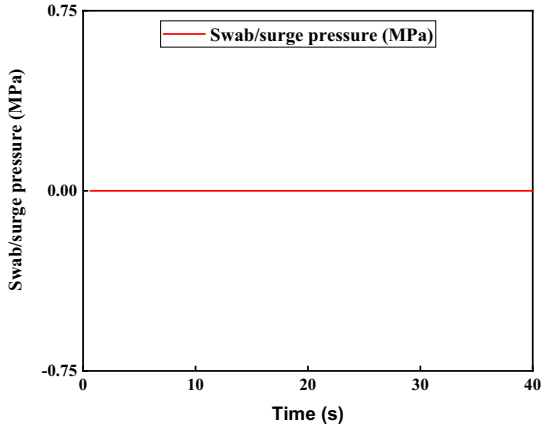

a) Without Swab and surge pressure

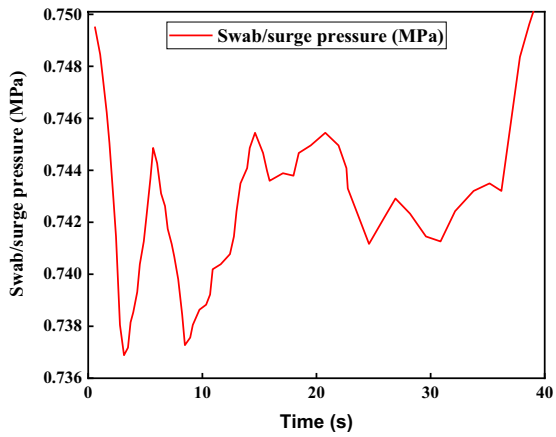

b) Maximal Swab and surge pressure P=0.75 MPa

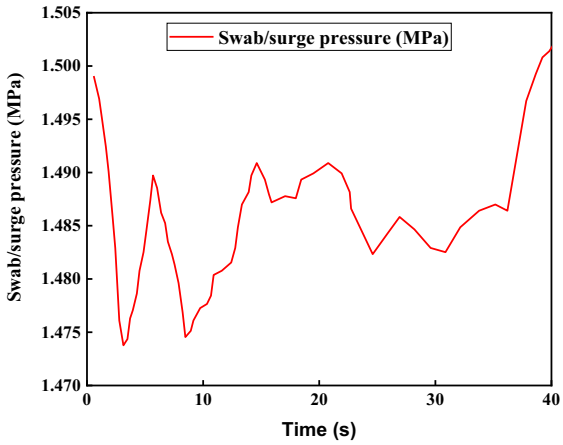

c) Maximal Swab and surge pressure P=1.5 MPa

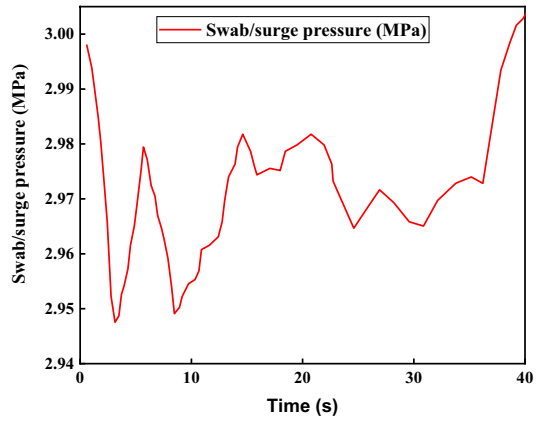

d) Maximal Swab and surge pressure P=3 MPa

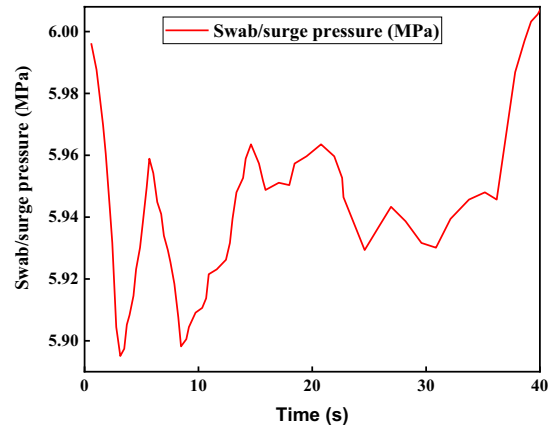

e) Maximal Swab/surge pressure P=6 MPa

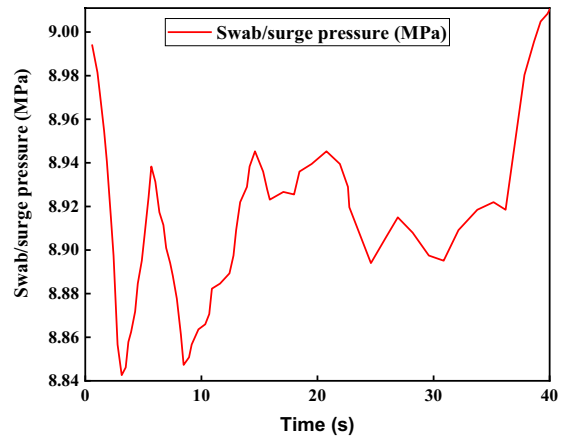

f) Maximal Swab/surge pressure P=9 MPa

Fig. 2 Swab and surge pressure loading cases used during the numerical modeling

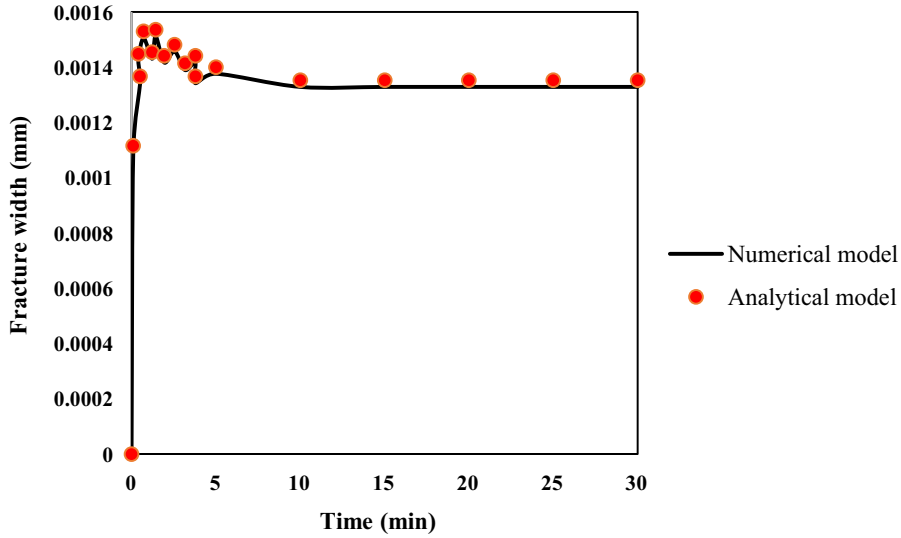

Fig. 3 Time evolution of fracture width near the wellbore fracture- mouth (K vertex) for Equivalent Circulating Density fluctuations caused by swab and surge pressure

The assumptions utilized in both the numerical and analytical modeling processes include:

- The rock formation is homogeneous, meaning that fracture toughness, Poisson's ratio (ν), and Young's modulus (E) have uniform values.
- The fracture is constructed with radially symmetric geometries.
- The gap between the fracture front and the fracturing fluid is considered insignificant.
- Fluid flow within the fracture adheres to a laminar and unidirectional regime.

Given these assumptions, the objective is to solve for key parameters such as:

1. The net fluid pressure (p), representing the disparity between the fluid pressure within the crack and the far-field stress.
2. The aperture of the fracture (w (x, t)), which varies both spatially (x) and temporally (t).
3. The half-length of the fracture (l(t)), indicating its extension along the spatial coordinate x, also changing with time (t).

4.2 Comparison between numerical and asymptotic solutions

In this study, the commercial software Abaqus is employed as the numerical simulator to conduct an analysis investigating the impact of swab and surge pressure on wellbore stability. However, before the results and conclusions derived from the numerical model can be considered reliable, it is crucial to validate the model's accuracy.

The validity of the numerical model is established through verification, wherein the disparity between numerical and analytical results of fracture length, fracture width, and pore fluid pressure is evaluated. Figures 3, 4 and 5 depict the comparison between asymptotic analytical solutions and numerical results for fracture aperture, fracture length, and fracture width distribution along the fracture. Similarly, Figs. 6 and 7 illustrate the correspondence between analytical and numerical solutions for pore fluid pressure and pore fluid distribution along the fracture. The comparison reveals a strong agreement between analytical and numerical solutions, thereby affirming the accuracy of the numerical results obtained using the newly developed numerical model.

5 Results and discussion of the analysis

5.1 Influence of the swab and surge pressure on the development of the wellbore natural fracture

This section outlines the outcomes concerning the impact of swab and surge pressure on three key aspects: the natural fracture development within the

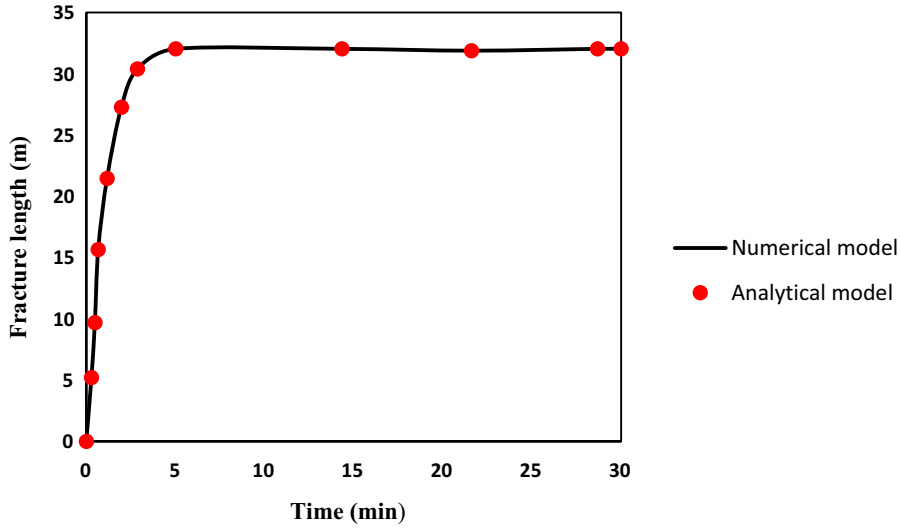

Fig. 4 Time evolution of fracture length near the wellbore fracture mouth (K vertex) for Equivalent Circulating Density fluctuations caused by swab and surge pressure

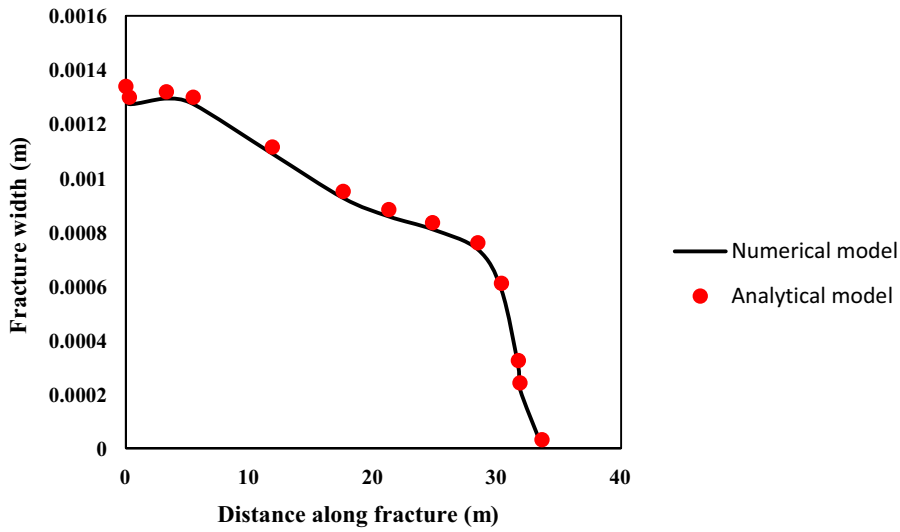

Fig. 5 Fracture width distribution along the fracture near the wellbore fracture mouth (K vertex) for Equivalent Circulating Density fluctuations caused by swab and surge pressure

wellbore, the rate of lost circulation, and the pore pressure.

5.1.1 Influence of the swab and surge pressure on the wellbore fracture width growth

In this section, the fracture-mouth width growth during mud circulation for different swab and surge pressure magnitude is investigated. It is observed in Fig. 8, that the fracture width on each profile increases with the swab and surge pressure magnitude. The maximal value of the fracture width without swab and surge pressure increased by 69.92% after application of swab and surge pressure with magnitude P = 9 MPa at the final stage of the simulation. Equally, the fracture width profiles increase with the swab and surge pressure magnitude during the mud circulation. In fact, the swab and surge pressure which is modeled as a distribution surface load directly applied on the wellbore surface causes an enlargement of the wellbore natural fracture. Therefore, the higher the swab and surge pressure magnitude, the larger the wellbore natural fracture width is observed during the numerical simulation. Other researches in the literature equally demonstrated the enlargement of the near wellbore natural

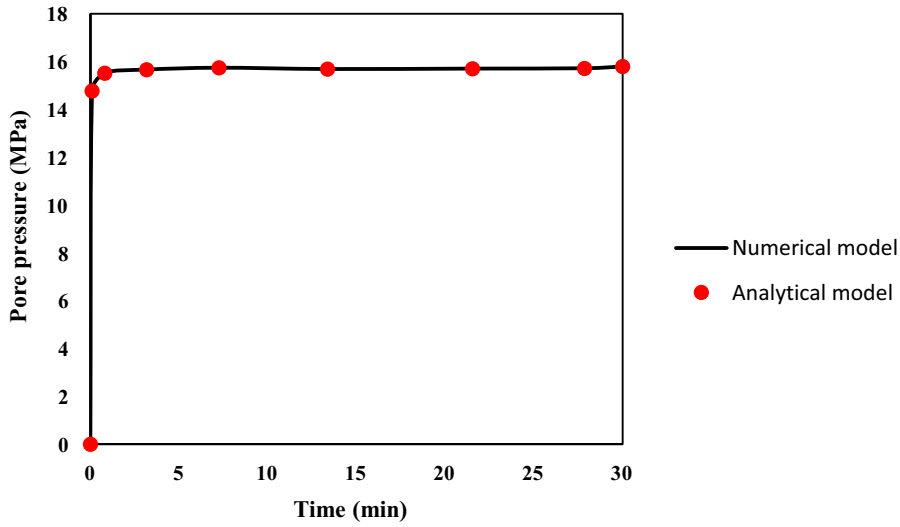

Fig. 6 Time evolution of pore pressure near the injection point (K vertex) for Equivalent Circulating Density fluctuations caused by swab/surge pressure

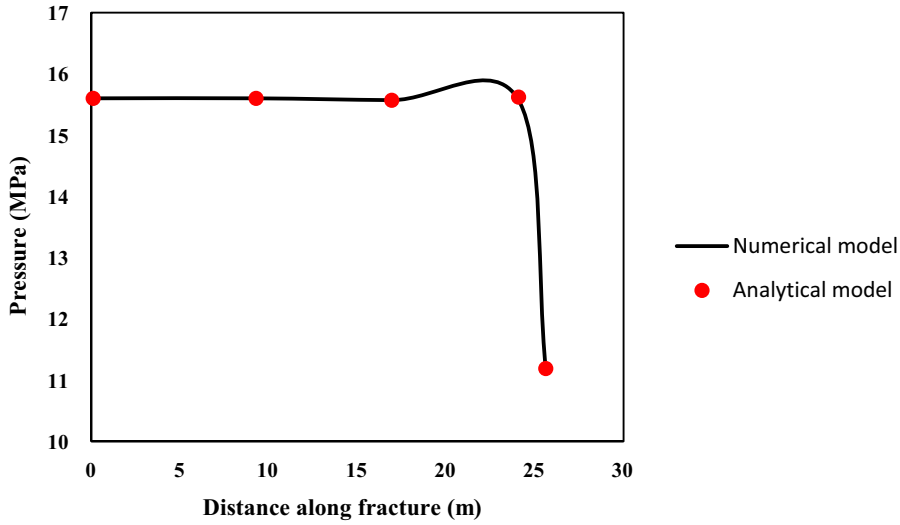

Fig. 7 Pore pressure distribution along fracture near the injection point (K vertex) for Equivalent Circulating Density fluctuations caused by swab and surge pressure

fracture width generated by the loads applied on the wellbore surface (Ewy et al. 2004; Khaled and Shokir 2017; Cerfontaine and Collin 2018). The accurate determination of the fracture width after integration of the swab and surge pressure will improve the determination of the particle size dimension required to seal the fractures and maintain the wellbore stability.

During the initial phase of the simulation (within the first 5 min), fluctuations in fracture width profiles occur due to the irregular development of fractures, aligning with observations made in the field by Morita et al. (1990), Raaen et al. (2001), and Ye et al. (2017). These fluctuations become more pronounced when swab and surge pressures are applied, causing the fracture to open and close in accordance with the fluctuations in pressure. This intensifies the oscillations in the fracture width profiles, as illustrated in Fig. 8.

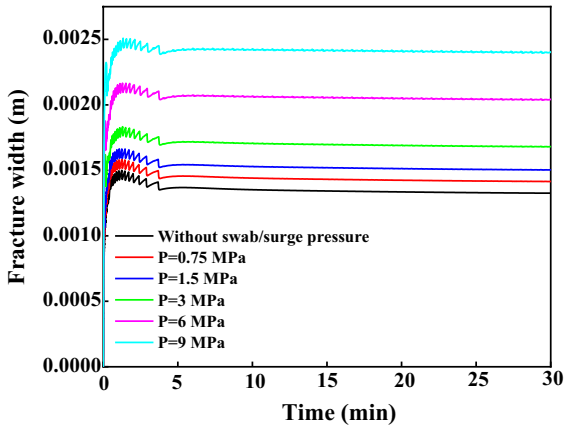

Fig. 8 Fracture width as a function of time profiles for different swab and surge pressure magnitude at the wellbore fracture mouth

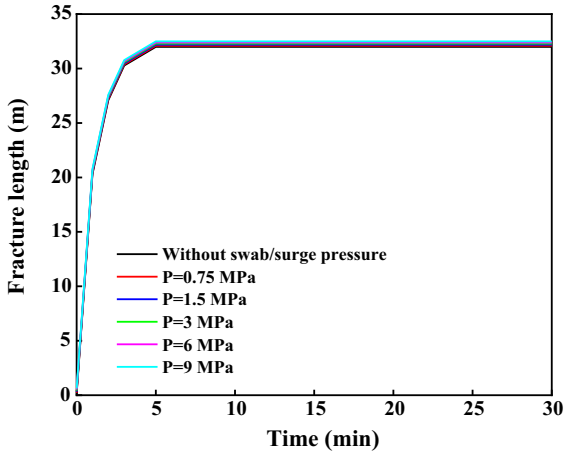

Fig. 9 Fracture length as a function of time profiles for different swab and surge pressure magnitude

5.1.2 *Influence of the swab and surge pressure on the wellbore fracture length growth*

This segment explores how swab and surge pressures affect the expansion of wellbore fracture length. In Fig. 9, the evolution of fracture length during mud circulation is depicted after applying varying magnitudes of swab and surge pressure.

It is observed that initially, the fracture length increases over time during the early stages of simulation, eventually stabilizing at a final length of 31.99 m. Interestingly, the introduction of swab and surge pressure does not significantly alter the fracture length profiles, suggesting that their impact is primarily confined to the vicinity of the wellbore surface. Consequently, while these pressures may widen the fracture near the wellbore, they do not notably contribute to further propagation of the fracture. However, to validate these findings, additional investigations are warranted, particularly with longer simulation times, as the current model is limited to a relatively short duration ($t = 30$ min).

5.1.3 *Fracture width versus fracture length for distinct swab and surge pressure*

Figure 10 illustrates the relationship between fracture width and fracture length under various swab and surge pressures. The investigation concludes that as the distance along the fracture increases, the width of the fracture diminishes. This phenomenon is attributed to the seepage of drilling fluid into the rock.

Furthermore, it is noted that the distribution of fracture width along the fracture increases as the magnitude of swab and surge pressure rises. This enlargement is primarily attributed to the fluctuating pressure applied to the wellbore surface, leading to an increase in near wellbore fracture width. Specifically, after applying a swab and surge pressure of 9 MPa, there's an observed 69.16% increase in fracture width near the wellbore region, compared to conditions without vibration.

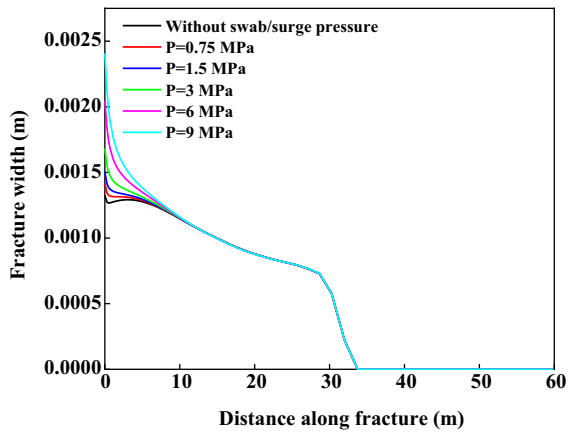

Fig. 10 Fracture width distribution along the fracture for different swab/surge pressure magnitude at the final stage of simulation ($t = 30$ min)

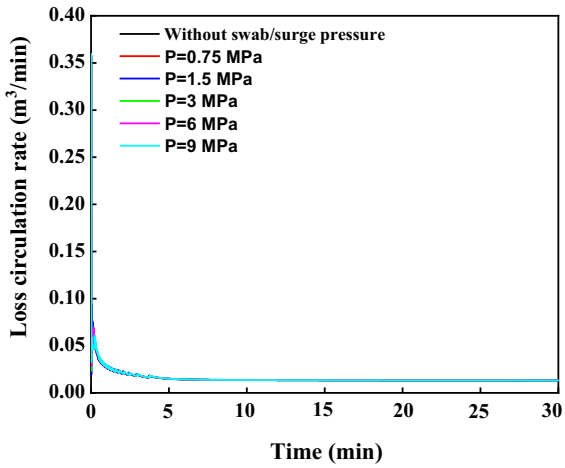

Fig. 11 Loss circulation rate during mud circulation for different swab and surge pressure magnitude at the wellbore fracture mouth

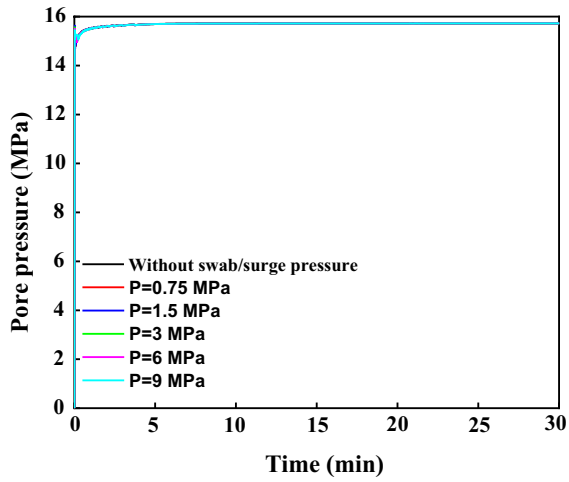

Fig. 12 Pore pressure as a function of time profiles for different swab and surge pressure magnitude at the wellbore fracture mouth

Additionally, it's observed that fracture width tends to be smaller near the wellbore, particularly evident in the scenario "without vibration." This phenomenon is attributed to stress concentration resulting from rock excavation at the onset of simulation, hindering the natural enlargement of fracture width. However, with the integration of swab and surge pressure, this stress concentration gradually diminishes. The pressure exerted on the wellbore surface aids in enlarging the natural fractures, relieving the stress concentration effect and allowing for wider fracture development.

5.1.4 Influence of the swab and surge pressure on the pore fluid pressure and the loss circulation rate

In drilling operations, minimizing mud loss volume is crucial. Therefore, assessing how Equivalent Circulating Density affects mud loss volume due to swab and surge pressure is of utmost importance. Figure 11 depicts the loss circulation rate at the mouth of the wellbore fracture during mud circulation under various magnitudes of swab and surge pressure. The findings indicate a sharp initial decrease in loss circulation rates over time, from 0.36 m^3/min to 0.033 m^3/min, attributed to fluid diffusion in the surrounding wellbore region. Moreover, it's observed that swab and surge pressure exert a weak influence on loss circulation rates. Despite variations in swab and surge pressure magnitudes, the mud loss volume remains relatively stable due to the low permeability of the rock formation utilized in the simulation and the localized effect of swab and surge pressure on the wellbore surface. Furthermore, the model is capable of evaluating pore fluid pressure at the fracture mouth over time, as illustrated in Fig. 12.

Significant pore pressure buildup is observed during the early stages of simulation ($t < 5$ min), rising from 0 MPa to 15.33 MPa due to extensive fluid diffusion at the wellbore surface. Subsequently, the pore pressure stabilizes around 15.45 MPa for later simulation periods. Interestingly, varying magnitudes of swab and surge pressure yield similar pore pressure profiles over time. This consistency arises because swab and surge pressure, modeled as mechanical surface loads, primarily impact fracture growth rather than pore fluid pressure. Additionally, the low permeability of the rock formation (5md) utilized in this research minimizes variations in pore pressure near the wellbore in response to swab and surge pressure.

In contrast, Zhang et al. (2018) explored the effect of transient swab and surge pressure on real-time wellbore stability evaluation and obtained contrasting results. Their study demonstrated that transient swab and surge pressure influenced pore fluid pressure in

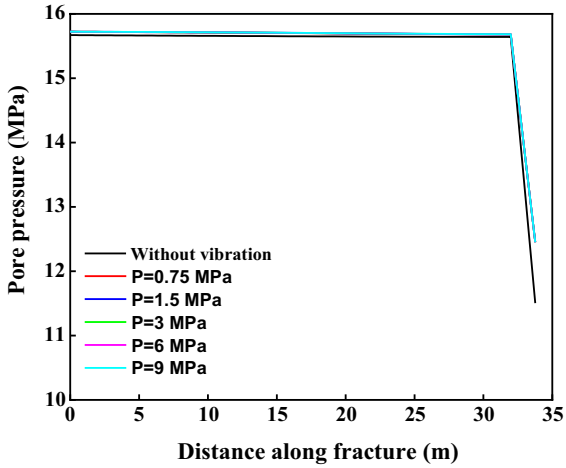

Fig. 13 Pore fluid pressure distribution within the fracture for different swab and surge pressure magnitude at the final stage simulation (t = 30 min)

the surrounding wellbore area, with its impact diminishing as distance from the wellbore increased. The disparity between these findings may stem from differences in rock permeability; this simulation utilized a lower permeability (5md) compared to Zhang et al.'s (2018) research (10 md). Furthermore, investigating the pressure of fluid within the fracture for varying swab and surge pressures is intriguing. Figure 13 depicts the results of fluid pressure within the fracture at the final stage of simulation.

The pore pressure remains consistent for a distance along the fracture less than 31.99 m. However, a notable pressure drop along the fracture is observed beyond this distance, corresponding to the point where fracture propagation ceases, as depicted in Fig. 5.2. Pore pressure profiles as a function of distance along the fracture exhibit a slight increase with swab and surge pressure magnitude. This is because varying surge pressures (0.75 MPa, 1.5 MPa, 3 MPa, 6 MPa, 9 MPa) force fluids into the fracture, elevating pressure. Consequently, this fluid movement alters the distribution of pore pressure along the fracture profile, leading to an overall increase in pore pressure. At the final stage of the simulation, the maximal value of pore pressure without swab and surge pressure experienced a 0.33% increase after applying a swab and surge pressure of magnitude P = 9 MPa.

Table 2 In-situ principal stresses for different stress faulting regimes

Stress regimes	In-situ principal stress		
	Vertical stress (MPa)	Max. horizontal stress (MPa)	Min. horizontal stress (MPa)
Normal faulting	22	19	17
Strike-slip faulting	22	24	18
Reverse faulting	22	26	24

5.2 Influence of the swab and surge pressure on the time-dependent safe mud window

Table 1 provides the details of the input parameters utilized in the simulation, encompassing information regarding the wellbore, rock formation, natural fracture, and drilling fluid. Meanwhile, Table 2 displays the in-situ principal stresses corresponding to various faulting stress conditions employed in the study.

5.2.1 Interaction between safe mud window and swab/ surge pressure

The mud window delineates the range of mud weights within which drilling the wellbore remains safe from instabilities. This window is defined by both a lower and an upper value. The lower value signifies the minimum mud weight necessary to prevent wellbore collapse, while the upper value indicates the maximum mud density to avert wellbore tensile failure. Figure 14 illustrates a comparison of the time-dependent safe mud window for wellbore stability, depicting scenarios with and without swab and surge pressure, specifically for a vertical wellbore under normal faulting stress conditions.

The study revealed that the mud window, initially stable, progressively narrowed over time following the introduction of swab and surge pressure. This outcome was anticipated because integrating swab and surge pressure resulted in fluctuations in Equivalent Circulating Density, consequently elevating near wellbore pore pressure.

The rise in pore pressure over time led to a continuous increase in collapse pressure and a decrease in fracture pressure, underscoring the significance

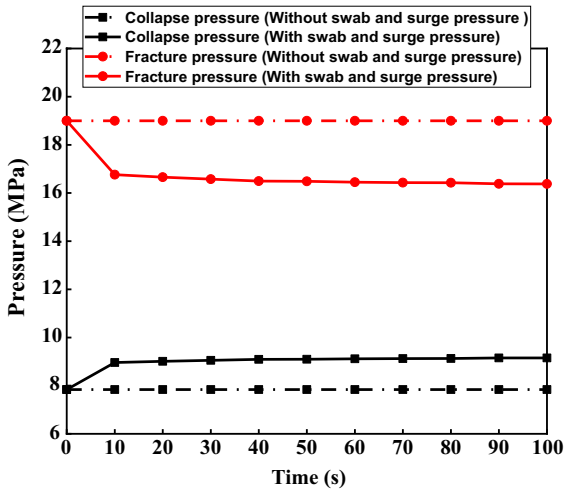

Fig. 14 Comparison of time dependent safe mud window with and without swab and surge pressure for borehole drilled in vertical direction in normal fault stress regime

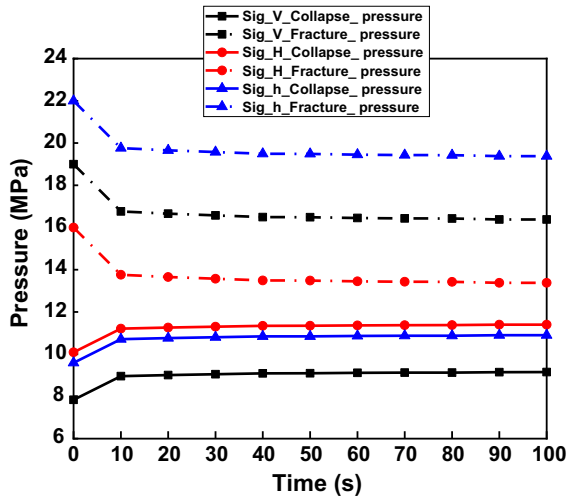

Fig. 15 Comparison of safe mud windows with swab and surge pressure for three wells orientation in normal faulting stress regime

of swab and surge pressure on the safe mud window. Without swab and surge pressure, collapse pressure and fracture pressure were measured at 7.84 MPa and 19 MPa respectively. Post-integration of swab and surge pressure, collapse pressure at the final simulation time increased by 14.33%, while fracture pressure decreased by 13.80%. Consequently, drilling mud initially within the safe region could transition into the unstable region after the integration of swab and surge pressure. Hence, relying on time-dependent safe mud weight is essential for accurate wellbore stability analysis.

These findings align with the conclusions drawn by Zhang et al. (2018), who similarly noted that incorporating swab and surge pressure in wellbore stability analysis resulted in a narrower mud weight window than initially anticipated. However, their focus was primarily on the impact of swab and surge pressure on near wellbore pore pressure.

5.2.2 *Influence of the stress faulting regimes and trajectory of the wellbore on the wellbore stability*

This section delves into examining the impact of stress faulting regimes and wellbore trajectory on wellbore stability. The investigation focuses on determining the safe mud weight windows for three different well orientations (vertical stress direction, maximum and minimum horizontal stress direction) across three faulting regimes. Figures 15, 16 and 17 depict a comparison of the safe mud windows with swab and surge pressure for the three well orientations, respectively, within the normal fault, strike-slip fault, and reverse fault regimes.

In the figures, "Sig_V," "Sig_H," and "Sig_h" respectively denote the vertical wellbore and wells

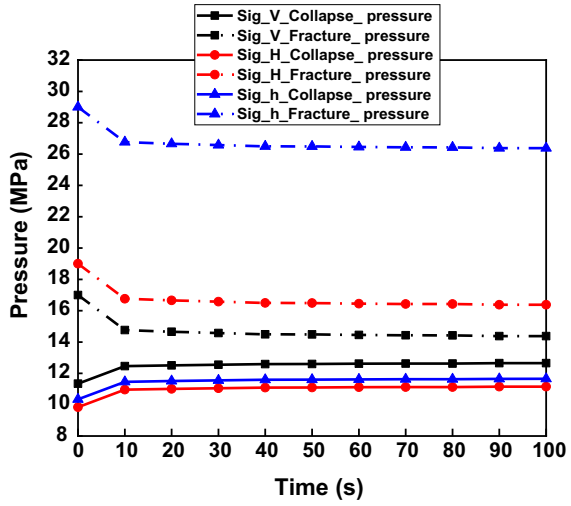

Fig. 16 Comparison of safe mud windows with swab and surge pressure for three wells orientation in strike-slip fault stress regime

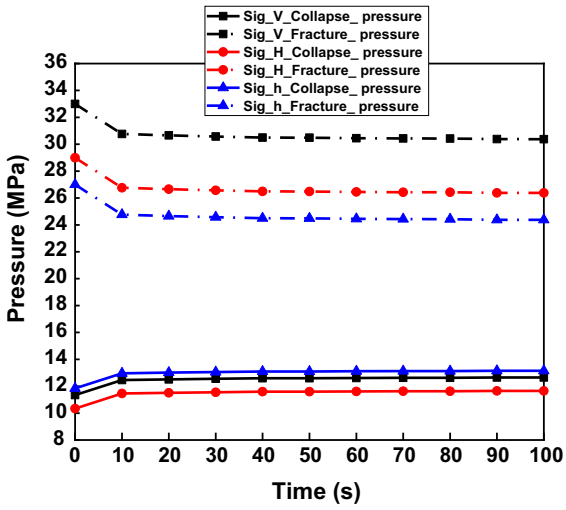

Fig. 17 Comparison of safe mud windows with swab and surge pressure for three wells orientation in reverse faulting stress regime

drilled in the maximal and minimal horizontal stress directions. Notably, for all cases, the safe mud windows progressively narrow over time. A wider mud window associated with the wellbore trajectory indicates increased stability during drilling operations. Additionally, maintaining mud density within the central range of the safe mud window ensures prolonged stability during the drilling process.

In the normal stress regime, the wellbore drilled horizontally parallel to the maximum in-situ stress exhibits the narrowest mud window (fracture pressure minus collapse pressure at the final simulation time is 1.98 MPa), while the wellbore drilled parallel to the lowest in-situ stress direction presents the widest mud window (fracture pressure minus collapse pressure at the final simulation time is 8.48 MPa), followed by the vertical wellbore. However, drilling in the direction parallel to the minimum in-situ stress necessitates the highest mud density for wellbore stability, while the vertical wellbore requires the lowest mud density.

In the strike-slip faulting regime, the well drilled in the direction parallel to the minimum in-situ stress consistently displays the widest mud window (gap between fracture pressure and collapse pressure at the final simulation time is 14.73 MPa), requiring the highest mud density to maintain stability. Conversely, the vertical wellbore is highly susceptible to instability due to its extremely narrow mud window (gap between fracture pressure and collapse pressure at the final simulation time is 1.73 MPa). However, the horizontal well parallel to the maximum in-situ stress requires the least mud weight for stability.

Within the reverse faulting regime, the wellbore in the vertical stress direction demands the highest drilling mud density and presents the largest mud window (gap between fracture pressure and collapse pressure at the final simulation time is 17.72 MPa), whereas the wellbore drilled parallel to the minimum in-situ stress exhibits the smallest mud window (gap between fracture pressure and collapse pressure at the final simulation time is 11.23 MPa). The wellbore drilled parallel to the maximum in-situ stress requires the least mud density to ensure stability.

Table 3 Effects of trajectory and stress faulting regimes on the time-dependent wellbore stability analysis

Stress-faulting regime	Widest mud window	Narrowest mud window	Well requiring the highest mud density to ensure wellbore stability	Well requiring the lowest mud density to ensure wellbore stability
Normal fault	Horizontal well drilled in the direction of the minimum horizontal stress	Horizontal well drilled in the direction of the maximum horizontal stress	Horizontal well drilled in the direction of the minimum horizontal stress	Vertical wellbore
Strike-slip fault	Horizontal well drilled in the direction of the minimum horizontal stress	Vertical wellbore	Horizontal well drilled in the direction of the minimum horizontal stress	Horizontal well drilled in the direction of the maximum horizontal stress
Reverse fault	Vertical wellbore	Horizontal well drilled in the direction of the minimum horizontal stress	Vertical wellbore	Horizontal well drilled in the direction of the maximum horizontal stress

Overall, the reverse faulting system requires the highest mud density for maintaining wellbore stability despite presenting a wider safe mud window, while the normal faulting regime demands the lowest mud density and presents the narrowest mud window. Consequently, for enhanced wellbore stability, drilling in the horizontal direction parallel to the minimum in-situ stress within the normal faulting regime emerges as the most suitable option. The impact of trajectory and stress faulting regimes on time-dependent wellbore stability analysis is summarized in Table 3.

6 Conclusion

In this study, the impact of swab and surge pressure on time-dependent wellbore stability was thoroughly investigated. Initially, the ABAQUS software was employed as a numerical simulator to analyze the effects of swab and surge pressure on wellbore natural fracture growth and time-dependent pore pressure. Subsequently, a MATLAB program was developed to assess the time-dependent safe mud window. To validate the numerical model, the obtained numerical results were compared with small asymptotic analytical solutions. The findings regarding the influence of swab and surge pressure on wellbore natural fracture development revealed several key points:

1. Fracture width increased proportionally with the magnitude of swab and surge pressure, with the maximal width without such pressure rising by 69.92% after application of a pressure magnitude of P = 9 MPa.
2. Fracture aperture decreased as fracture length increased due to fluid leakage into neighboring rock. A 69.16% increase in fracture width was observed in the near wellbore region after applying a swab and surge pressure magnitude of P = 9 MPa.
3. Fracture length, loss circulation rate, and pore fluid pressure remained relatively unchanged post-integration of swab and surge pressure, primarily impacting the wellbore surface due to low rock permeability.
4. Pore pressure along fracture profiles increased with swab and surge pressure magnitude, with the maximal value increasing by 0.33% after applying a pressure magnitude of P = 9 MPa.
5. The initially constant safe mud window narrowed over time after integration of swab and surge pressure. Collapse pressure increased by 14.33%, while fracture pressure decreased by 13.80% at the final simulation time.
6. For various wellbore trajectories and stress faulting scenarios, safe mud windows equally narrowed with time evolution.

Furthermore, the effect of swab and surge pressure on the time-dependent safe mud window was examined, leading to the following conclusions:

The newly developed model accurately predicts natural fracture growth, loss circulation rate, and pore pressure under fluctuating wellbore pressures caused by swab and surge pressure. These results are valuable for wellbore strengthening studies aimed at determining optimal particle size dimensions to plug natural fractures and mitigate lost circulation during drilling operations. Additionally, the model precisely determines the safe mud window under swab and surge pressure, crucial for maintaining wellbore stability during drilling operations.

7 SI metric conversion factors

cp	×1.0 *	10^{-3}	=	Pa·s
in	×2.54 *	10^{-2}	=	m
md	×9.869233	10^{-16}	=	m^2

[2] * conversion factor is exact.

Acknowledgements This research was funded by the National Natural Science Foundation of China project research NO. 51774050 and the Open Fund of Hubei Key Laboratory of Oil and Gas Drilling and Production Engineering of Yangtze University (grant recipient : Dr Kamgue Lenwoue Arnaud Regis).

Declarations

Conflict of interest The authors declare that they have no known competing financial interests or personal relationships that could have appeared to influence the work reported in this paper.

References

Abduljabbar AM, Hossain E, AlGharbi S, & Al-Rubaii M (2018) Optimization of Tripping speed to minimize Surge& Swab pressure. Paper presented at the SPE/IADC Middle east drilling technology conference and exhibition held in Abu Dhabi. 29–31 Jan.SPE-189331-MS. https://doi.org/10.2118/189331-MS

Bergeron L (1961) Water hammer in hydraulics and wave surges in electricity, 1st edn. Wiley, New York

Bunger AP, Detournay E, Garagash DI (2005) Toughness-dominated hydraulic fracture with leak-off. Int J Fract 134:175–190. https://doi.org/10.1007/s10704-005-0154-0

Burkhadt JA (1961) Pressures surges produced by pipe movement. J Petrol Technol 13(06):595–605. https://doi.org/10.2118/1546-G-PA

Cannon GE (1934) Changes in hydrostatic pressures due to withdrawing drill pipe from the hole. Drill Prod Prac AP I:42

Cerfontaine B, Collin F (2018) Cyclic and fatigue behaviour of rock materials: review, interpretation and research perspectives. Rock Mech Rock Eng 51:391–414. https://doi.org/10.1007/s00603-017-1337-5

Churchill SW (1977) Friction factor equation spans all fluid-flow regimes. Chem Eng 84:91–92

Crespo F, Ahmed R, Enfis M, Saasen A, Amani M (2012) Surge-and-swab pressure predictions for yield-power-law drilling fluids. SPE Drill Compl 27(04):574–585. https://doi.org/10.2118/138938-PA

Chen B, Barron AR, Owen DR, Li CF (2018) Propagation of a plane strain hydraulic fracture with a fluid lag in permeable rock. J Appl Mech 85(9):091003

Ewy RT, Bovberg CA, Chen G, Jansson R and Pepin G (2004) Fatigue testing of hollow cylinders and application to injection well cycling. 5–9 June.ARMA/NARMS 04–464. In: Proceedings of the Gulf Rocks 2004, the 6th north America rock mechanics symposium, Houston, TX, USA

Feng Y, Gray EK (2018a) Modeling lost circulation through drilling induced fractures. SPE J 23(01):205–223. https://doi.org/10.2118/187945-PA

Feng Y, & Gray KE (2018) Effects of porous properties of rock on near-wellbore hydraulic fracture complexity. Paper presented at the unconvetional resources technology conference, Houston, Texas, USA, 23–25 Jul.urtec:2883153. https://doi.org/10.15530/urtec-2018-2883153

Feng Y, Gray KE (2018c) modeling lost circulation through drilling-induced fractures. SPE J 23:205–223. https://doi.org/10.2118/187945-pa

Fjar E, Holt RM, Raaen AM, Risnes R, Horsrud P (2008) Petroleum related rock mechanics, 2nd edn. Elsevier, Amsterdam

Fontenot JE, Clark RK (1974) An improved method for calculating swab and surge pressures and circulating pressures in a drilling well. SPE J. https://doi.org/10.2118/4521-PA

Garagash DI (2006) Plane-strain propagation of a fluid-driven fracture during injection and shut-in: asymptotics of large toughness. Eng Fract Mech 73:456–481. https://doi.org/10.1016/j.engfracmech.2005.07.012

Goins WC, Weichert JP, Burba JL (1951) Down- the- hole pressures surges and their effect on loss of circulation drilling and production practices. American Petroleum Institute, Washington

Horn AJ (1950) Well blowouts in California Drilling operations causes and suggestions for prevention. In: Drilling and production practices, 112–128. Washington, American Petroleum Institute

Hu J, Garagash DI (2010) Plane-strain propagation of a fluid-driven crack in a permeable rock with fracture toughness. J Eng Mech 136:1152–1166. https://doi.org/10.1061/(asce)em.1943-7889.0000169

Jaeger JC, Cook NG, Zimmerman R (2009) Fundamentals of rock mechanics. Wiley, Hoboken

Khaled MS, Shokir EM (2017) Effect of drillstring vibration cyclic loads on wellbore stability. In: Proceedings of the SPE middle east oil & gas show and conference. Manama, Kingdom of Bahrain

Kong X, Lin Y, Qiu Y, Zhu H, Dong L, Chen Y (2014) A new model for predicting dynamic surge pressure in gas and drilling mud two-phase flow during tripping operations. Math Probl Eng 2014(916798):1–16. https://doi.org/10.1155/2014/916798

Lal M (1983) Surge and Swab modeling for dynamic pressures and safe trip velocities. In: Paper presented at the IADC/SPE drilling conference, New Orleans, Louisiana, USA, 20–23. SPE-11412-MS. https://doi.org/10.2118/11412-MS

Liu W, Zhou B, Li Y, Yu B, & Deng J (2018) numerical analysis of wellbore instability in weakly consolidated rock formations. In: Paper presented at the ISRM international symposium—10th Asian rock mechanics symposium, Singapore, 29 Oct–03 Nov. ISRM-ARMS10–2018–136

Lubinski A, Hsu FH, Nolte KG (1977) Transient pressure surges due to pipe movement in an oil well. Revue De L'inst Franç Du Pét 32(3):307–348

Meng M, Zamanipour Z, Miska S, Yu M, Ozbayoglu E (2019b) Dynamic stress distribution around the wellbore influenced by surge/swab pressure. J Pet Sci Eng 172:1077–1091. https://doi.org/10.1016/j.petrol.2018.09.016

Meng M, Zamanipour Z, Miska S, Yu M, Ozbayoglu EM (2019a) Dynamic wellbore stability analysis under tripping operations. Rock Mech Rock Eng 52:3063–3083. https://doi.org/10.1007/s00603-019-01745-4

Mitchell RF (1988) Dynamic surge/swab pressure predictions. SPE Drill Eng 3(3):325–333. https://doi.org/10.2118/16156-PA

Morita N, Black AD, Guh G-F (1990) Theory of lost circulation pressure. In: SPE annual technical conference exhibition. New Orleans. 23–26 Sept. SPE 20409

Osisanya S (2010) Practical approach to solving wellbore instability problems. SPE Distinguished lecturer program. doi: www.spe.org/go/DL50

Peirce A, Detournay E (2008) An implicit level set method for modeling hydraulically driven fractures. Comput Methods Appl Mech Eng 197:2858–2885. https://doi.org/10.1016/j.cma.2008.01.013

Raaen AM, Skomedal E, Kjorholt H et al (2001) Stress determination from hydraulic fracturing tests. Int J Rock Mech Min Sci 38:529–541

Rahman MK, Naseby D, Rahman SS (2000) Borehole collapse analysis incorporating time-dependent pore pressure due to mud penetration in shales. J Pet Sci Eng 28(2000):13–31

Samuel GR, Sunthankar A, McColpin G, Bern P, Flynn T, & Sun S (2001) Field validation of transient swab/surge response with PWD data. Paper presented at the IADC/SPE drilling conference held in Amsterdam, Netherlands, 27 Feb–01 Mar. SPE-67717-MS. doi:https://doi.org/10.2118/67717-MS

Samuel GR, Sunthankar A, McColpin G, Bern P, Flynn T, Sun S (2003) Field validation of transient swab/surge response with PWD data. SPE Drill Compl 18(04):280–283. https://doi.org/10.2118/85109-PA

Savitski A, Detournay E (2002) Propagation of a penny-shaped fluid-driven fracture in an impermeable rock: asymptotic solutions. Int J Solids Struct 39:6311–6337. https://doi.org/10.1016/s0020-7683(02)00492-4

Schuh FJ (1964) Computer makes surge-pressure calculations useful. Oil Gas J 3(31):96

Simulia (2016) Abaqus version 2016. Analysis user's guide. Providence, Rhode Island, USA. Dassault Systemes

Sneddon IN, Lowengrub M (1969) Crack problems in the classical theory of elasticity. Wiley, New York

Srivastav R, Enfis M, Crespo F, Ahmed R, Saasen A, & Laget M (2012) Surge and swab pressures in horizontal and inclined wells. In: Paper presented for the SPE Latin America and Caribbean petroleum engineering conference, 16–18, Mexico City, Mexico. https://doi.org/10.2118/152662-MS

Tang M, Xiong J, He S (2014) A new model for computing surge/swab pressure in horizontal wells and influencing factors. J Nat Gas Sci Eng 19:337–343. https://doi.org/10.1016/j.jngse.2014.05.026

Tikhonov V, Bukashkina O, Liapidevskii V, & Ring L (2016) Development of model and software for simulation of surge-swab process at drilling. In: Paper presented at the SPE Russian petroleum technology conference and exhibition held in Moscow. Russia, 24–26 Oct. SPE-181933-MS. https://doi.org/10.2118/181933-MS

Wu R, Deng J, Liu W, &, et al (2018) Numerical investigation of fluid injection into poorly consolidated into poorly con-solidated geomaterial considering shear dilation and compaction. J Pet Sci Eng 168:119–132. https://doi.org/10.1016/j.petrol.201

Ye Z, Janis M, Ghassemi A et al (2017) Experimental investigation of injection-driven shear and slip and permeability evolution of granite for EGS stimulation. In: 42 nd workshop on geothermal reservoir engineering. Standford, California

Zamanipour Z, Miska SZ, & Hariharan PR (2016) Effect of transient surge pressure on stress distribution around directional wellbores. In: Paper presented at the IADC/SPE drilling conference and exhibition, Fort Worth, Texas, USA, 1–3 Mar. SPE-178831-MS. doi: https://doi.org/10.2118/178831-MS

Zhang F, Kang Y, Wang Z, Miska S, Yu M, Zamanipour Z (2018) Transient coupling of swab/surge pressure and in situ stress for wellbore stability evaluation during tripping. SPE J 23(04):1019–1038. https://doi.org/10.2118/180307-PA

Zielonka MG, Searles KH, Ning J, & Buechler SR (2014) Development and validation of fully-coupled hydraulic fracturing simulation capabilities. In: SIMULIA community conference, Providence, Rhode Island